



## Experiment Report Form

**The double page inside this form is to be filled in by all users or groups of users who have had access to beam time for measurements at the ESRF.**

Once completed, the report should be submitted electronically to the User Office via the User Portal:  
<https://www.esrf.fr/misapps/SMISWebClient/protected/welcome.do>

### Deadlines for submission of Experimental Reports

Experimental reports must be submitted within the period of 3 months after the end of the experiment.

#### Experiment Report supporting a new proposal (“relevant report”)

If you are submitting a proposal for a new project, or to continue a project for which you have previously been allocated beam time, you must submit a report on each of your previous measurement(s):

- even on those carried out close to the proposal submission deadline (it can be a “*preliminary report*”),
- even for experiments whose scientific area is different from the scientific area of the new proposal,
- carried out on CRG beamlines.

You must then register the report(s) as “relevant report(s)” in the new application form for beam time.

### Deadlines for submitting a report supporting a new proposal

- 1<sup>st</sup> March Proposal Round - **5<sup>th</sup> March**
- 10<sup>th</sup> September Proposal Round - **13<sup>th</sup> September**

The Review Committees reserve the right to reject new proposals from groups who have not reported on the use of beam time allocated previously.

#### Reports on experiments relating to long term projects

Proposers awarded beam time for a long term project are required to submit an interim report at the end of each year, irrespective of the number of shifts of beam time they have used.

#### Published papers

All users must give proper credit to ESRF staff members and proper mention to ESRF facilities which were essential for the results described in any ensuing publication. Further, they are obliged to send to the Joint ESRF/ ILL library the complete reference and the abstract of all papers appearing in print, and resulting from the use of the ESRF.

Should you wish to make more general comments on the experiment, please note them on the User Evaluation Form, and send both the Report and the Evaluation Form to the User Office.

### Instructions for preparing your Report

- fill in a separate form for each project or series of measurements.
- type your report in English.
- include the experiment number to which the report refers.
- make sure that the text, tables and figures fit into the space available.
- if your work is published or is in press, you may prefer to paste in the abstract, and add full reference details. If the abstract is in a language other than English, please include an English translation.



	<b>Experiment title:</b> Multiscale structure – performance relations in printed polymeric materials	<b>Experiment number:</b> A26-2-952
<b>Beamline:</b> BM 26	<b>Date of experiment:</b> from: 18 <sup>th</sup> January, 2023 to: 23 <sup>rd</sup> January, 2023	<b>Date of report:</b>
<b>Shifts:</b> 15	<b>Local contact(s):</b> Martine Rosenthal	<i>Received at ESRF:</i>
<b>Names and affiliations of applicants</b> (* indicates experimentalists):  <b>Francisco Molina-Lopez (Department of Materials Engineering (MTM), KU Leuven, Belgium)</b> <b>*Tzu-Yi Yu (Department of Materials Engineering (MTM), KU Leuven, Belgium)</b> <b>*Bokai Zhang (Department of Materials Engineering (MTM), KU Leuven, Belgium)</b> <b>*Tanmay Sinha (Department of Materials Engineering (MTM), KU Leuven, Belgium)</b>		

**Report:**



## **ESRF experiment report**

**Beamline:** BM26

**Project:** CRG – DUBBLE

**Experiment time:** 18<sup>th</sup> – 23<sup>rd</sup> April 2023

**Main proposer:**

- **Francisco Molina-Lopez** (Department of Materials Engineering (MTM), KU Leuven, Belgium)

**Participant:**

- **Tzu-Yi Yu** (Department of Materials Engineering (MTM), KU Leuven, Belgium)
- **Bokai Zhang** (Department of Materials Engineering (MTM), KU Leuven, Belgium)
- **Tanmay Sinha** (Department of Materials Engineering (MTM), KU Leuven, Belgium)

**Local contact:**

- **Martin Rosenthal**

## **Introduction**

Wearable devices are integrating high-end technologies such as smart medical treatment, real-time health monitoring, and human-robot interfaces into our daily lives. However, energy storage and harvesting remain challenging for the development of these devices. Polymer-based energy harvesting devices such as organic thermoelectric generators (OTEGs) and photovoltaics (OPVs) offer promising solutions due to their biocompatibility, materials abundance, and outstanding mechanical flexibility. Despite their performance often being inferior to that of inorganic materials, tuning the polymer morphology has been shown to boost its performance. Therefore, the microstructural characterization or electronic polymers and its correlation to device performance are crucial topics for OTEs and OPVs.

Printing techniques allow for the fabrication of organic materials into flexible devices/modules while also enabling the tuning of their microstructure to boost performance. For example, the solution-shearing method can induce anisotropic morphology in PEDOT: PSS thin film, leading to a boost of OTE performance up to 5 times. (Hinckley, 2021) Mechanical rubbering and drawing can also induce anisotropic morphology in polymer films, enhancing their OTE performance. (Scheunemann, 2020) Brush printing is a technique commonly used for patterning continuous thin films and has been shown to provide a reliable approach to induce alignment in various types of conducting polymers. (Wang, 2017). Therefore, our goal for printed OTE materials is to promote morphological anisotropy by tuning the printing parameters. Two printing techniques are used here to prepare OTE materials with uniaxially-aligned morphology in both through- and in-plane direction: the direct ink writing (DIW) 3D-printing technique and brush printing. By tuning printing parameters, we expect to improve the structural alignment and performance in printed bulk and thin-film materials and, meanwhile, offer manufacturing flexibility for various device geometries.

We use the inkjet printing method to prepare films for OPVs. Inkjet printing offers the advantages of being contactless, additive, digital, and maskless. This allows quick and precise patterning and reduces waste during printing. The morphology of the active layer, known as the bulk heterojunction (BHJ), plays an important role in OPV efficiency, as reported in the literature. For instance, face-on and end-on orientations have been reported to be desirable for OPVs and light-emitting diodes that require high levels of out-of-plane transport. (Müller-Buschbaum, 2014; Pandey, 2019) The fast-drying of inkjet-printed films, made up of tiny drops, allows us to access a wide range of new morphologies that can boost the performance of OPV. (Chen, 2022) Additionally, we aim to

tune the morphology of the device by developing co-solvent systems and optimizing the annealing temperature of the printed films.

## Experimental methods

In this experiment we tested four types of materials; they are 1) OTE bulk materials produced by direct-ink-writing (DIW), 2) OTE thin films produced by brush-printing, and 3) OPV thin films produced by ink-jet printing. The substrate for the thin film samples is silicon. The OTE bulk materials are characterized by small-angle and wide-angle X-ray scattering (SAXS/WAXS), and the thin films are tested by grazing incident small-angle and wide-angle X-ray scattering (GISAXS/GIWAXS). All the data are collected by a Pilatus 1M detector with a 12 keV X-ray. The details of the data processing are described in the results and discussion sections.

## Results and discussion

- **3D-printed (DIW) OTE**

To induce molecular alignment and boost the thermoelectric performance of organic materials, we applied a shearing force during the direct-ink-writing (DIW) process. In this experiment, we prepared several printed PEDOT:PSS "pillars" using nozzles of varying sizes and characterized them using wide-angle X-ray scattering (WAXS). We also used filtration pre-treatment and solvent vapor post-treatment to enhance the thermoelectric performance of PEDOT:PSS "pillars". We examined the morphological changes resulting from pre- and post-treatment using WAXS.

In the first experiment, we studied the morphological changes resulting from pre- and post-treatment of PEDOT:PSS pillars. The filtration pre-treatment involved washing the PEDOT:PSS aqueous solution with excessive DMSO and vacuum-assisted filtration before ink preparation. This approach efficiently removes excessive PSS in the solution, which is an insulating component in the material. The reduced WAXS data of samples with (red lines) and without (blue lines) filtration pre-treatment are shown in **Figure 1**. Comparing the signal of PSS ( $q \sim 1.3 \text{ \AA}^{-1}$ ) and PEDOT ( $q \sim 1.8 \text{ \AA}^{-1}$ ), we confirmed that filtration pre-treatment increases the PEDOT/PSS ratio. Furthermore, filtration pre-treatment leads to a more compact packing of PEDOT in the  $\pi$ - $\pi$  direction, causing the PEDOT  $\pi$ - $\pi$  signal ( $q \sim 1.8 \text{ \AA}^{-1}$ ) to shift to a higher  $q$  value. These morphological changes are beneficial to enhancing the electrical conductivity of PEDOT:PSS.

On the other hand, we applied solvent vapor treatment to further enhance the thermoelectric performance of PEDOT:PSS after printing. We freeze-dried the PEDOT:PSS pillars to maintain their shape and post-treated them with ethanol vapor in a closed environment overnight. In contrast to filtration pre-treatment, solvent vapor post-treatment did not result in a significant  $\pi$ - $\pi$  stacking intensity increase but contributed to slightly shifting the peak further to the right for filtered samples, representing a closer spacing between PEDOT backbones. Also, PEDOT lamellar stacking ( $q \sim 0.25 \text{ \AA}^{-1}$ ) massively increased after post-treatment for filtered samples. No significant difference was observed for non-filtered samples after solvent post-treatment. The reduced WAXS data of samples before (solid lines) and after (dashed lines) solvent vapor post-treatment are shown in **Figure 1**.

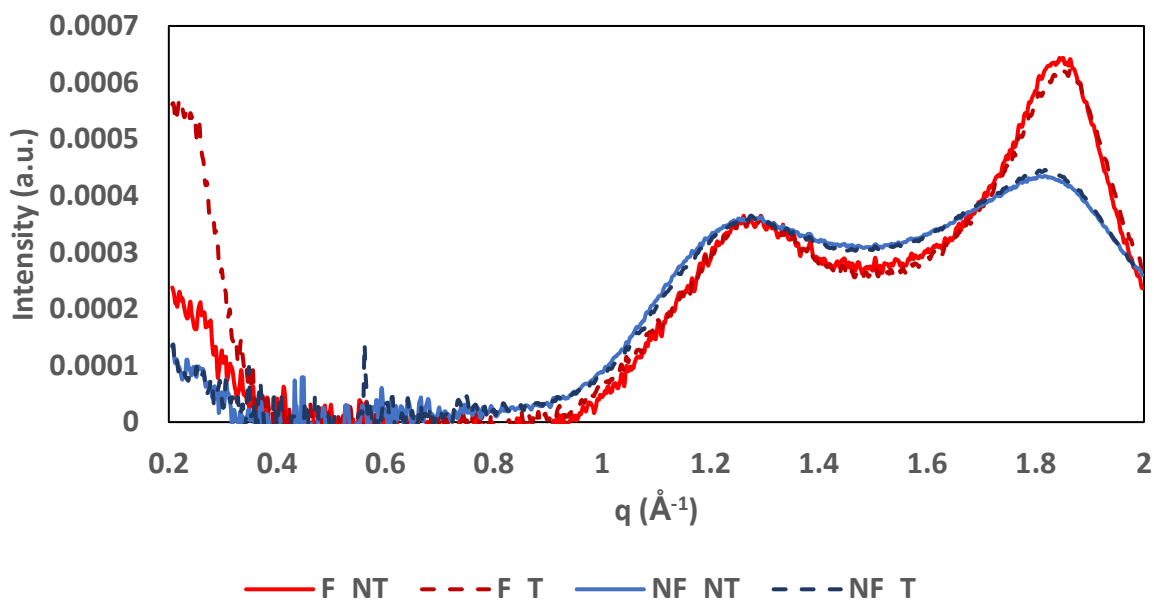


**Figure 1** 1D reduced WAXS signal of DIW-printed PEDOT:PSS pillars. F (or NF) indicates that the PEDOT:PSS ink is treated (or not treated) with filtration pre-treatment. T (or NT) indicates that the sample is post-treated (or not) with solvent vapor. Filtration pre-treatment has a dominant effect on increasing PEDOT  $\pi$ - $\pi$  stacking ( $q \sim 1.8 \text{ \AA}^{-1}$ ) and slightly promoting PEDOT lamellar stacking ( $q \sim 0.25 \text{ \AA}^{-1}$ ). Solvent vapor treatment has a minor effect on morphological change, but dramatically induces PEDOT lamellar stacking ( $q \sim 0.25 \text{ \AA}^{-1}$ ) for filtration pre-treated samples. The results are normalized by the PSS signal.

In our project, the effect of nozzle size is critical because it determines the shearing force on PEDOT:PSS ink during the direct-ink-writing (DIW) process. A strong shearing force is expected to induce a more organized and uniaxially-aligned PEDOT crystal structure, which can improve the thermoelectric performance of the material. In **Figure 2**, we present the 1D reduced WAXS data of pillars printed by different nozzle heads, denoted as L, M, and S for large, medium, and small nozzle heads, respectively. Our WAXS results show that using a small nozzle head promotes a more ordered structure of the PEDOT crystal. Specifically, the peak of PEDOT  $\pi$ - $\pi$  stacking ( $q \sim 1.8 \text{ \AA}^{-1}$ ) is narrowed, and the PEDOT lamellar signal ( $q \sim 0.25 \text{ \AA}^{-1}$ ) is increased when the sample is prepared using a small nozzle head. Notably, the position of these peaks remains unchanged across the different nozzle sizes, indicating that the nozzle size only improves the order of the PEDOT crystal without altering its intermolecular distance ( $\pi$ - $\pi$  stacking).

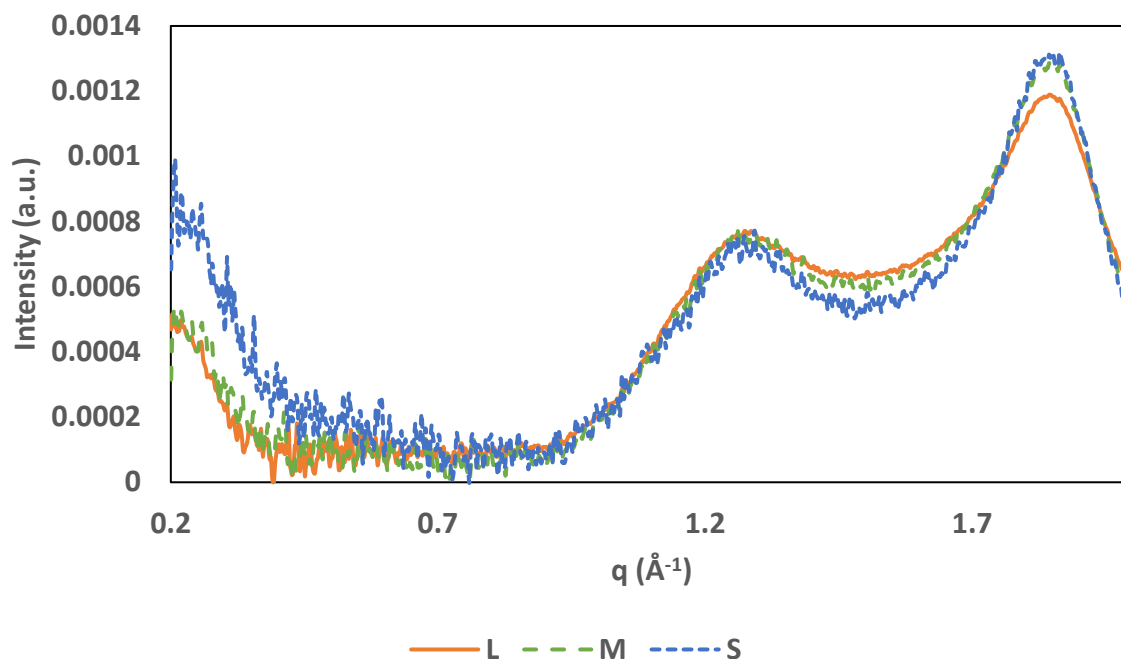


**Figure 2** 1D reduced WAXS signal of DIW-printed PEDOT:PSS pillars. All the samples are prepared by filtration pre-treated PEDOT:PSS ink and post-treated by solvent vapor treatment. L, M, and S indicate the sample is printed with a large, medium, and small nozzle, respectively. A small nozzle head induces a more organized PEDOT crystalline phase, including more PEDOT lamella stacking ( $q \sim 0.25 \text{ \AA}^{-1}$ ) and PEDOT crystallites with higher coherence length (narrower and  $\pi$ - $\pi$  stacking peak at  $q \sim 1.8 \text{ \AA}^{-1}$ ). The PEDOT  $\pi$ - $\pi$  stacking distance does not change with nozzle size. The results are normalized by the PSS signal.

To summarize, the filtration pre-treatment significantly enhances the PEDOT-to-PSS ratio and improves the order structure of the PEDOT crystal, and solvent vapor treatment further enhances the PEDOT packing in pre-treated PEDOT:PSS samples. As for the nozzle size, using a small nozzle head induces a more ordered PEDOT crystal structure in both the lamella and  $\pi$ - $\pi$  directions. By combining filtration pre-treatment, solvent vapor post-treatment, and a small printing head, we can obtain a PEDOT:PSS pillar with a high PEDOT/PSS ratio and an ordered PEDOT crystalline structure, which should result in high thermoelectric performance.

- **Brush-printed OTE**

In this experiment, we prepare PEDOT:PSS thin films on a silicon wafer by brush-printing. The microstructure of these films is characterized by GIWAXS from two directions, parallel and perpendicular to the brushing direction, as shown in **Figure 3(a)**. By comparing the signal from parallel and perpendicular directions, we can study the morphological difference and polymer alignment of brush-printed films. During the last GIWAXS experiment, we found that PEDOT:PSS brush-printed at a speed of 3mm/s exhibits the best PEDOT alignment toward the brushing direction and the highest electrical conductivity. Herein, we study the post-treatment effect on the PEDOT:PSS film prepared under 3mm/s brushing speed.

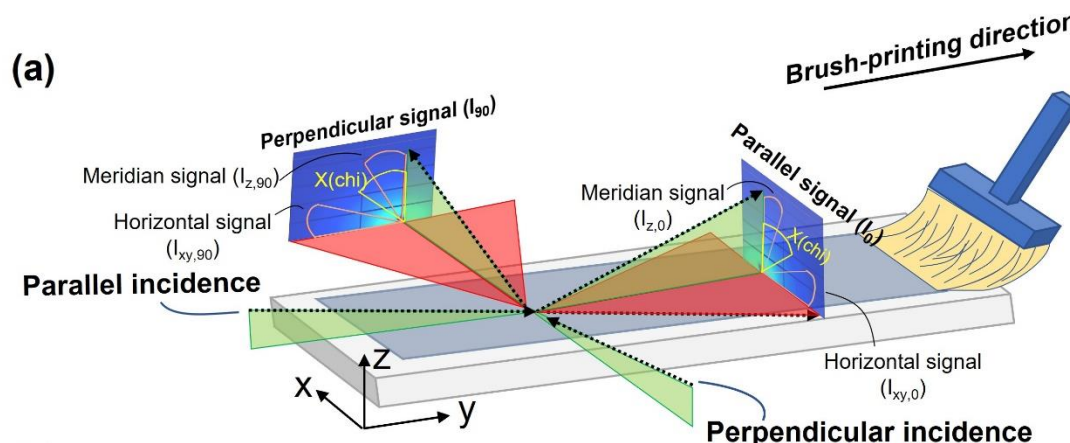


**Figure 3** (a) Sketch of the fabrication of brush-printed film and its GIWAXS characterization from two directions concerning the brush-printing direction.

Solvent post-treatment is a typical method to increase the thermoelectric performance of PEDOT:PSS films. (G-H. Kim, 2014) Also, meniscus-based technique can be combined with solvent post-treatment to induce an anisotropic morphology. (Hinckley, 2021) In this experiment, we study the microstructural change after treating brush-printed PEDOT:PSS film with DMSO by two methods, dropping solvent on the film or brushing the film with solvent (referred to as uniaxially post-treatment). Before solvent post-treatment (noted as “Pristine” in **Figure 4**), the brush-printed PEDOT:PSS film already presents different microstructures in parallel and perpendicular directions. Besides the sharp ring signals at high  $q$  from unknown contamination in the perpendicular direction, we find a broad ring around  $q = 15 \text{ nm}^{-1}$  that is credited to PSS. (**Figure 4(b)**) On the other hand, two distinct rings located around  $q = 15$  and  $18 \text{ nm}^{-1}$  can be found in the parallel direction. (**Figure 4(a)**) The one around  $q = 18 \text{ nm}^{-1}$  is assigned as PEDOT  $\pi$ - $\pi$  stacking signal. Because  $\pi$ - $\pi$  signal can be found more obviously in the parallel direction, we can expect that PEDOT crystals are partially aligned toward the brushing direction. After treating PEDOT:PSS film by dropping DMSO on its top to remove excess of PSS, the PSS signal in both directions (**Figure 4(c),(d)**) is indeed significantly reduced but the PEDOT  $\pi$ - $\pi$  stacking signal remains stronger along the parallel direction than along the perpendicular direction. Moreover, the intensity of the horizontal part of the ring is now much stronger now than the meridian, suggesting that the PEDOT crystals transferred from face-on orientation into edge-on orientation upon DMSO drop post-treatment. Compared to drop post-treatment, the PEDOT:PSS film treated by solvent-shearing method resulted in further enhanced contrast in the PEDOT peak brightness between parallel and perpendicular directions, indicating stronger alignment. As a matter of fact, the PEDOT (PSS) signal can be found only in the parallel (perpendicular) direction.

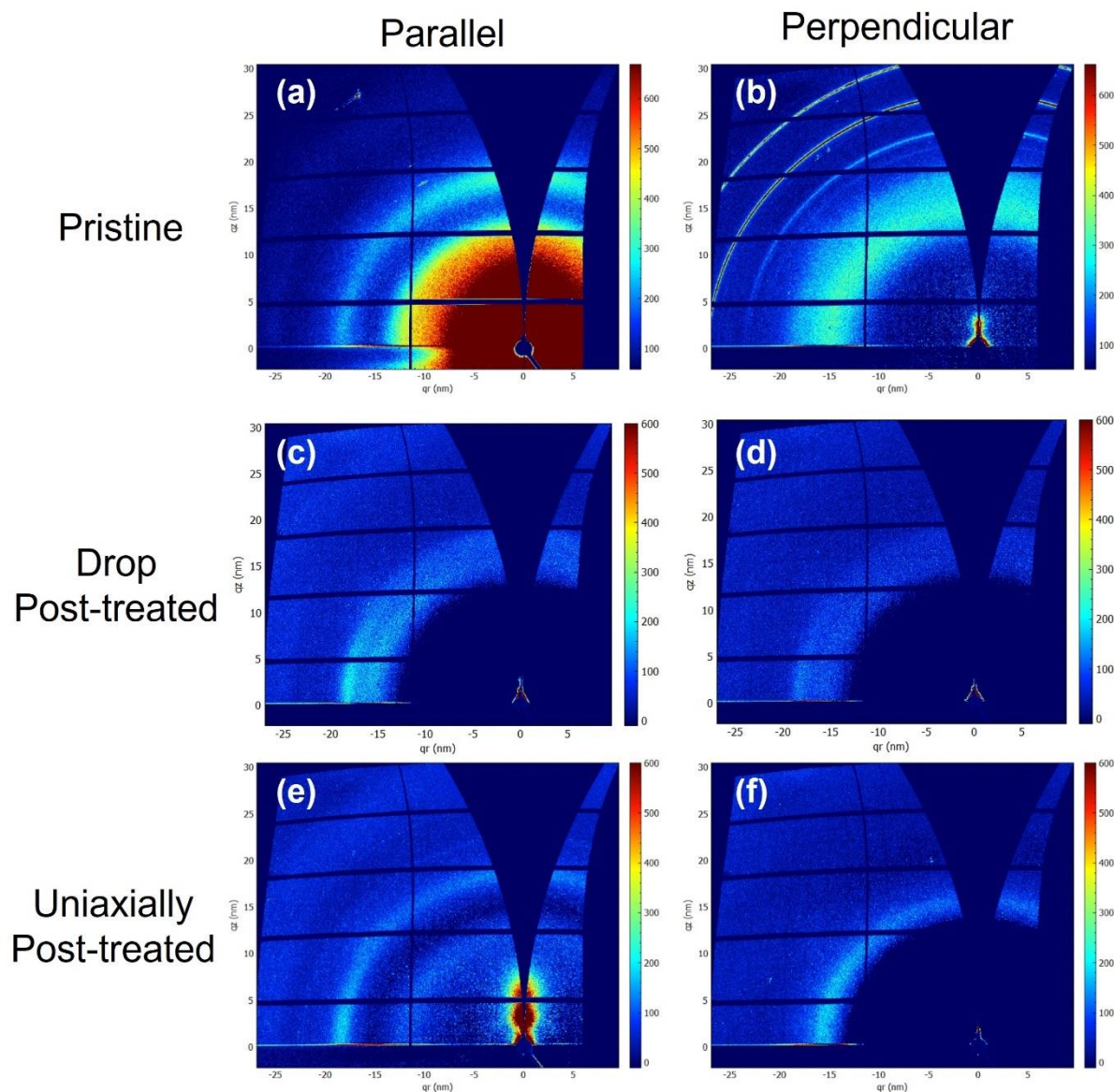


**Figure 4** 1D reduced WAXS result of brush-printed PEDOT:PSS films. The PEDOT:PSS brush-printed films are probed from parallel and perpendicular direction, respectively. Two post-treatment methods are respectively applied to study their resulting morphological changes.

To summarize, pristine brush-printed PEDOT:PSS films display uniaxial alignment along the printing direction. DMSO post-treatment is effective in removing PSS and promoting edge-on orientation. Moreover, compared to the drop casting post-treatment, the uniaxial post-treatment method further enhances the anisotropic contrast. These morphological changes, i.e. uniaxial alignment, reduced fraction of PSS and edge-on orientation, are expected to enhance the mobility of the films, and hence their thermoelectric performance compared to the pristine films.

- **Ink-jet printed OPV**

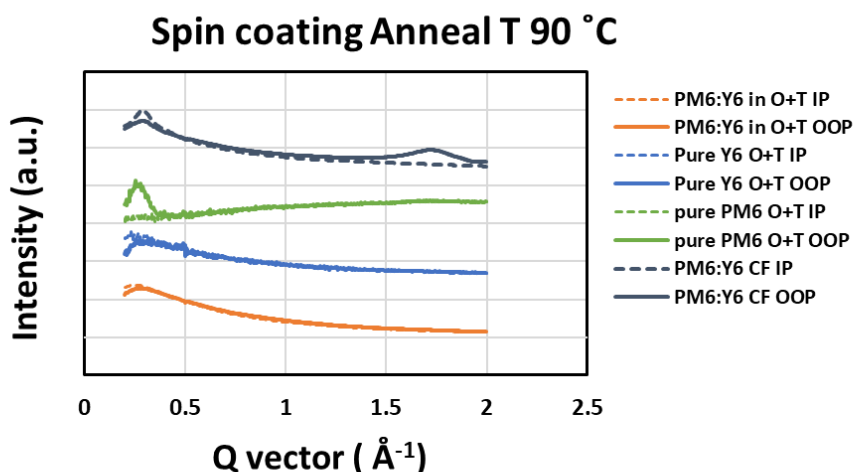
The performance of OPVs relies largely on the morphology of its active layer, which can be influenced by various fabrication parameters, including the solvent (McDowell, 2018), the substrate, temperature (Wang Z. G., 2021), film preparation methods, and so on. In this study, we aim to investigate the morphology of the active layer samples by comparing the neat phase film and blend film in different solvent systems listed in **Table 1**, neat film with different fabrication parameter such as inkjet printing

plate temperature and post-annealing temperature listed in **Table 2**, PM6:Y6 blend film with different printing plate temperature and post-annealing temperature listed in **Table 3**. In our active layer film, we chose PM6:Y6 blend film as this polymer composite in an OPV device has been reported to have high performance, reaching PCE maximum to 28.8% under indoor light condition (Kuen, 2020). We will further correlate our GIWAXS results to OPVs performance.

**Table 1.** Spin-coated (SC) active layer blend film and neat films in co-solvent system and blend film in chloroform

Sample name	Fabrication method	Material	Solvent	Plate temperature (°C)	Annealing temperature (°C)
Pure PM6	SC	PM6	O-xylene + 5% tetralin	RT	90
Pure Y6	SC	Y6	O-xylene + 5% tetralin	RT	90
PM6:Y6	SC	PM6:Y6	O-xylene + 5% tetralin	RT	90
PM6:Y6 CF	SC	PM6:Y6	Chloroform	RT	90

PM6:Y6, PM6, and Y6 in o-xylene: tetralin (95%/5%, v/v) co-solvent spin-coated films are prepared to compare with the spin-coated PM6:Y6 in chloroform reference film. Spin-coated samples of PM6 exhibit lamellar stacking  $q \sim 0.29 \text{ \AA}^{-1}$  in the out-of-plane, while Y6 shows no crystalline signals. The results also point out that different solvents affect the film's crystallinity as we compared the PM6:Y6 blend film in co-solvent system and chloroform. Spin-coated samples of PM6:Y6 in chloroform showed a strong lamellar signal at  $q \sim 0.29 \text{ \AA}^{-1}$  and  $\pi$ - $\pi$  stacking signals at  $q \sim 1.7 \text{ \AA}^{-1}$  in the out-of-plane region. The results of spin-coated blend film in chloroform is consistent with the literature (Kuen et al. 2020). In contrast, both lamellar and  $\pi$ - $\pi$  stacking signals can hardly be found in all the co-solvent blend sample. The 1D reductions of 2D GIWAXS patterns after background subtraction are shown in **Figure 5**. The solid lines represent spin-coated samples in out-of-plane, and the dashed lines represent samples in in-plane direction. The absence of the  $\pi$ - $\pi$  stacking signal in co-solvent system indicates that the solvent choice plays a crucial role in the crystallization behavior of the PM6:Y6 blend.



**Figure 5** 1D GIWAXS results of PM6:Y6, PM6, and Y6 films prepared by spin-coating in o-xylene: tetralin (95%/5% v/v) and PM6:Y6 in chloroform. The peak at  $q \sim 0.29 \text{ \AA}^{-1}$  represents lamellar stacking and  $q \sim 1.7 \text{ \AA}^{-1}$  represents the  $\pi$ - $\pi$  stacking.

The solvents have different properties, which can influence the molecular packing and mobility of the polymer chains within the film. In the case of *o*-xylene and tetralin, the lower polarity and higher boiling point of the solvent may hinder the formation of ordered domains, resulting in a lack of crystalline signal in the GIWAXS data. On the other hand, chloroform has a higher polarity and lower boiling point, which seems to promote the formation of ordered domains and more efficient molecular packing, leading to the observed lamellar and  $\pi$ - $\pi$  stacking signals.

**Table 2.** Inkjet printing (IJP) samples of neat films in co-solvent with different plate temperature and post-annealing temperature

Sample name	Fabrication method	Material	Solvent	Plate temperature (°C)	Annealing temperature (°C)
PM6 RT_60°C	IJP	PM6	O-xylene + 5% tetralin	RT	60
PM6 RT_90°C	IJP	PM6	O-xylene + 5% tetralin	RT	90
PM6 40°C_60°C	IJP	PM6	O-xylene + 5% tetralin	40	60
Y6 RT_60°C	IJP	Y6	O-xylene + 5% tetralin	RT	60
Y6 RT_90°C	IJP	Y6	O-xylene + 5% tetralin	RT	90
Y6 40°C_60°C	IJP	Y6	O-xylene + 5% tetralin	40	60

Inkjet printing PM6 and Y6 neat films are prepared to clarify whether fabricate our films under different plate temperature and post-annealing temperature conditions will affect the crystallinity. Neat PM6 films show clear lamellar stacking at  $q \sim 0.29 \text{ \AA}^{-1}$  in out-of-plane. The results show that both increasing the plate temperature during inkjet printing and post-annealing temperature will increase the crystallinity: In Y6 neat films, only raising the post-annealing temperature increases  $\pi$ - $\pi$  stacking signals whereas the lamellar signal of PM6 increases more significantly with increasing temperature. The 1D reductions of 2D GIWAXS patterns after background subtraction are shown in **Figure 6**. The solid lines represent samples in out-of-plane, and the dashed lines represent samples in in-plane. The crystallization behavior observed in the GIWAXS data can be related to molecular mobility that facilitates the formation of ordered domains. This effect is more prominent for PM6.

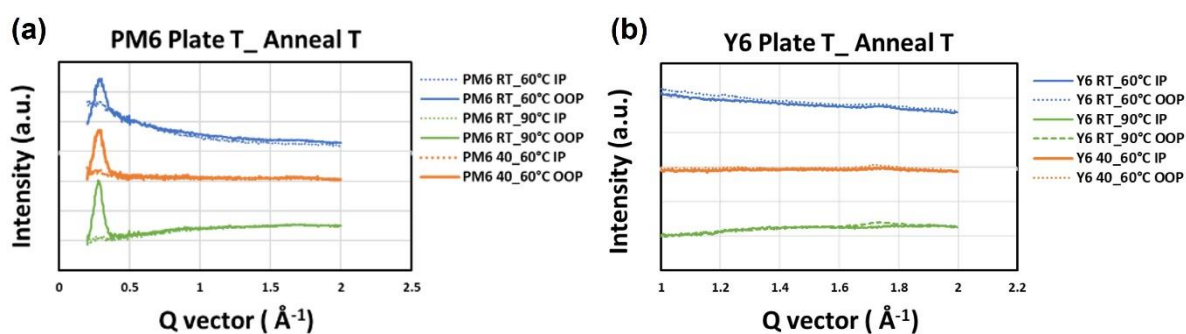


**Figure 6** 1D GIWAXS results of (a) PM6 and (b) Y6 films prepared by inkjet printing under different fabrication plate temperature and annealing temperature. The ink solutions are prepared by dissolving PM6 or Y6 in *o*-xylene: tetralin (95%/5% v/v).

**Table 3** Inkjet printing (IJP) samples of PM6:Y6 in co-solvent with different plate temperature and post-annealing temperature

Sample name	Material	Solvent	Plate temperature (°C)	Annealing temperature (°C)
-------------	----------	---------	------------------------	----------------------------

PM6:Y6 Plate RT_RT	PM6:Y6	O-xylene + 5% tetralin	RT	RT
PM6:Y6 Plate RT_60°C	PM6:Y6	O-xylene + 5% tetralin	RT	60
PM6:Y6 Plate RT_90°C	PM6:Y6	O-xylene + 5% tetralin	RT	90
PM6:Y6 Plate RT_120°C	PM6:Y6	O-xylene + 5% tetralin	RT	120
PM6:Y6 Plate 40°C_RT	PM6:Y6	O-xylene + 5% tetralin	40	RT
PM6:Y6 Plate 40°C_60°C	PM6:Y6	O-xylene + 5% tetralin	40	60
PM6:Y6 Plate 40°C_90°C	PM6:Y6	O-xylene + 5% tetralin	40	90
PM6:Y6 Plate 40°C_120°C	PM6:Y6	O-xylene + 5% tetralin	40	120

After examining both PM6 and Y6 neat films, we proceeded to conduct our experiment in PM6:Y6 blend film with different plate temperature and post-annealing temperature. The 1D reductions of 2D GIWAXS patterns after background subtraction are shown in **Figure 7**. The solid lines represent spin-coated samples in out-of-plane, and the dashed lines represent samples in in-plane direction. From the result, the GIWAXS data for PM6:Y6 in o-xylene and tetralin co-system did not show any crystalline signals, indicating that the material is amorphous. The absence of crystalline signals was observed even after varying the fabrication temperature and post-annealing temperature. This could be attributed to the presence of solvent molecules, which prevent the alignment of polymer chains into a crystalline structure. The results suggest that further studies using different solvents or different ratio of the co-solvent are necessary to explore the crystalline behavior of the material.

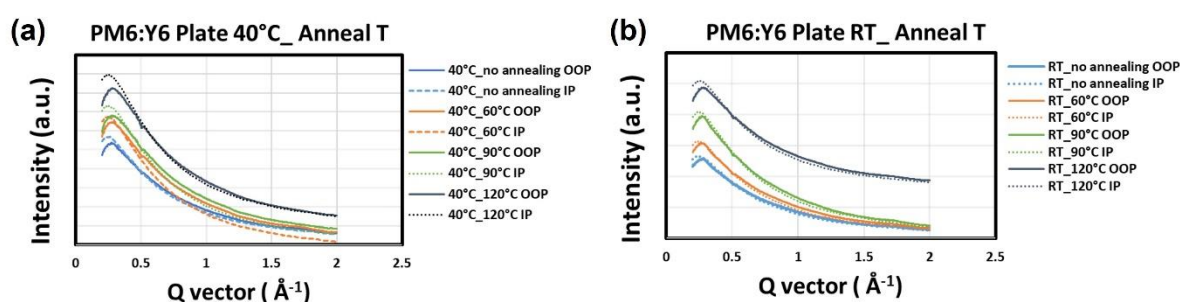


**Figure 7** 1D GIWAXS results of PM6:Y6 films prepared on (a) 40°C and (b) room temperature substrates followed by thermal annealing under varied temperature. The films are prepared by inkjet printing, and the ink solution is prepared by dissolving PM6:Y6 in o-xylene: tetralin (95%/5% v/v).

## Conclusion

The obtained (GI)WAXS results of printed OTEs provide insight into morphological changes resulting from different pre- and post-treatments. For the DIW PEDOT:PSS pillars, the filtrated PEDOT:PSS ink shows a significant enhancement in the PEDOT/PSS ratio and a more organized PEDOT crystalline phase. The post-treatment of solvent vapor results in a further enhancement of the PEDOT packing. Furthermore, the nozzle size in the DIW process controls the microstructure of PEDOT crystalline as well, where the small nozzle provides a long-range order of PEDOT  $\pi$ - $\pi$  stacking. By combining the filtration pre-treatment, solvent vapor post-treatment, and a small nozzle in the DIW process, we can obtain a highly ordered PEDOT crystalline which should lead to great thermoelectric performance.

Post-treatment brings a different morphological change to brush-printed PEDOT:PSS films. DMSO post-treatment is an efficient way to increase PEDOT/PSS ratio of brush-printed films. By combining the DMSO post-treatment and brushing process, we can enhance the anisotropy of the ratio PEDOT/PSS. Such a uniaxial post-treatment provides a way to control the anisotropic morphology of printed OTE films.

To optimize the morphology of the active layer in OPVs, we prepared several samples for GIWAXS to investigate the crystallinity of the PM6, Y6 neat film and PM6:Y6 blend films under

different fabrication methods, solvent systems, and temperature conditions. The results of PM6:Y6 blend film showed strong lamellar and  $\pi$ - $\pi$  stacking in chloroform, however, it shows nearly no packing performance in the o-xylene and tetralin co-solvent system. Another experiment data shows that with the rise of operating temperature and post-annealing temperature, the crystallinity of neat films mildly increases. However, inkjet printing PM6:Y6 blend films did not show any significant difference with the temperature change. Both solvent choice and temperature tuning play a crucial role in regulating the crystallization behavior of polymer blends. Therefore, in future experiments, we could consider using different solvent ratios combinations and investigate their impact on the crystallization behavior.

### Future work

From this beamtime, we obtain a great amount of data that helped us understand the morphological changes of printed OTE/OPV according to the given processing methods and guide a way to optimize their performance. We are trying to link the polymer microstructure from (GI)WAXS results with their material properties. In the future, we plan to optimize the materials' properties and, in the meanwhile, explore more approaches to boost their performance. Our final goals are to push the OTE/OPV performance beyond the reported records and to demonstrate their flexible devices on soft substrates.

### References

- Angmo, D. L.-O. (2013). Roll-to-roll inkjet printing and photonic sintering of electrodes for ITO free polymer solar cell modules and facile product integration. . *Adv. Energy Mater.*, 172–175.
- Brabec, C. J. (2008). Solution-processed organic solar cells. *MRS Bull*, 670–675.
- Chen, S. P. (2020). Unraveling vertical inhomogeneity in vapour phase polymerized Pedot:TOS films. *Journal of Materials Chemistry*, 18726-18734.
- Chen, X. H. (2022). Balancing the molecular aggregation and vertical phase separation in the polymer: Nonfullerene blend films enables 13.09% efficiency of organic solar cells with Inkjet-Printed Active Layer. *Advanced Energy Materials*, 2200044.
- Cutting, C. L., & Venkataraman, D. (2016). Indoor Light Recycling: A new home for organic photovoltaics. *Journal of Materials Chemistry C*, 10367–10370.
- G-H. Kim, L. S. (2014). Engineered doping of organic semiconductors for. *Nature Materials*.
- Gu, X. Y.-L. (2016). Comparison of the morphology development of polymer-fullerene and polymer-polymer solar cells during solution-shearing blade coating. *Advanced Energy Materials*, 1601225.
- Hinckley, A. C. (2021). Achieving high thermoelectric performance and metallic transport in solvent-sheared PEDOT:PSS. *Advanced Electronic Materials*.
- Kuen, L. M. (2020). High-Efficiency Indoor Organic Photovoltaics with a Band-Aligned Interlayer. *Joule*, 4(7), 1486–1500.
- Lu, L. e. (2015). Recent Advances in Bulk Heterojunction Polymer Solar Cells. *Chem. Rev.*, 12666–12731 .

- Ma, L.-K. C. (2020). High-efficiency indoor organic photovoltaics with a band-aligned interlayer. *Joule*, 1607–1611.
- McDowell, C. A. (2018). Solvent Additives: Key Morphology-Directing Agents for Solution-Processed Organic Solar Cells. *Advanced Materials*, 30(33), 1707114.
- Molina-Lopez, F. W. (2018). Enhancing molecular alignment and charge transport of solution-sheared semiconducting Polymer Films by the electrical-blade effect. *Advanced Electronic Materials*.
- Müller-Buschbaum, P. (2014). The active layer morphology of organic solar cells probed with grazing incidence scattering techniques. *Advanced Materials*, 7692–7709.
- Nozariasbmarz, A. S. (2020). Thermoelectric generators for wearable body heat harvesting: Material and device concurrent optimization. *Nano Energy*, 104265.
- Pandey, M. K. (2019). Recent advances in the orientation of conjugated polymers for organic field-effect transistors. *Journal of Materials Chemistry C*, 13323–13351.
- Scheunemann, D. V. (2020). Rubbing and drawing: Generic Ways to improve the thermoelectric power factor of organic semiconductors? *Advanced Electronic Materials*, 2000218.
- Shi, W. S. (2017). Tuning thermal transport in chain-oriented conducting polymers for Enhanced Thermoelectric Efficiency: A computational study. *Advanced Functional Materials*, 1702847.
- Wang, G. H. (2017). Aggregation control in natural brush-printed conjugated polymer films and implication for enhancing charge transport. *Proceedings of the National Academy of Science*.
- Wang, Z. G. (2021). The coupling and competition of crystallization and phase separation, correlating thermodynamics and kinetics in OPV morphology and performance. *Nature Communication*, 12(1).
- Wei, Q. M. (2014). Experimental studies on the anisotropic thermoelectric properties of conducting polymer films. *ACS Macro Letters*, 948–952.
- Zhu, L. Z. (2020). Efficient organic solar cell with 16.88% efficiency enabled by refined acceptor crystallization and morphology with improved charge transfer and transport properties. *Advanced Energy Materials*, 1904234.